Physica Medica 84 (2021) 1–9

Contents lists available at ScienceDirect

Physica Medica

journal homepage: www.elsevier.com/locate/ejmp

Original paper

Ultra-low dose whole-body CT for attenuation correction in a dual tracer PET/CT protocol for multiple myeloma

Elena Prieto [a,b], María José García-Velloso [b,c,*], Jesús Dámaso Aquerreta [b,d], Juan José Rosales [c], Juan Fernando Bastidas [c], Ignacio Soriano [d], Leticia Irazola [a], Paula Rodríguez-Otero [b,e], Gemma Quincoces [b,c], Josep María Martí-Climent [a,b]

[a] Medical Physics, Clínica Universidad de Navarra, Pamplona, Spain
[b] IdisNA, Instituto de Investigación Sanitaria de Navarra, Pamplona, Spain
[c] Nuclear Medicine, Clínica Universidad de Navarra, Pamplona, Spain
[d] Radiology, Clínica Universidad de Navarra, Pamplona, Spain
[e] Hematology, Clínica Universidad de Navarra, Pamplona, Spain

ARTICLE INFO

Keywords:
PET/CT
Radiation dose
Optimization
Multiple myeloma

ABSTRACT

Purpose: To investigate within phantoms the minimum CT dose allowed for accurate attenuation correction of PET data and to quantify the effective dose reduction when a CT for this purpose is incorporated in the clinical setting.

Methods: The NEMA image quality phantom was scanned within a large parallelepiped container. Twenty-one different CT images were acquired to correct attenuation of PET raw data. Radiation dose and image quality were evaluated.

Thirty-one patients with proven multiple myeloma who underwent a dual tracer PET/CT scan were retrospectively reviewed. ^{18}F-fluorodeoxyglucose PET/CT included a diagnostic whole-body low dose CT (WBLDCT: *120 kV-80mAs*) and ^{11}C-Methionine PET/CT included a whole-body ultra-low dose CT (WBULDCT) for attenuation correction (*100 kV-40mAs*). Effective dose and image quality were analysed.

Results: Only the two lowest radiation dose conditions (*80 kV-20mAs* and *80 kV-10mAs)* produced artifacts in CT images that degraded corrected PET images. For all the other conditions ($CTDI_{vol} \geq 0.43$ mGy), PET contrast recovery coefficients varied less than $\pm$ 1.2%.

Patients received a median dose of 6.4 mSv from diagnostic CT and 2.1 mSv from the attenuation correction CT. Despite the worse image quality of this CT, 94.8% of bone lesions were identifiable.

Conclusion: Phantom experiments showed that an ultra-low dose CT can be implemented in PET/CT procedures without any noticeable degradation in the attenuation corrected PET scan. The replacement of the standard CT for this ultra-low dose CT in clinical PET/CT scans involves a significant radiation dose reduction.

Introduction

Although the use of PET/CT has rapidly increased worldwide since the development of hybrid imaging [1,2], radiation exposure can be a thoughtful concern due to the ionizing nature of both PET and CT [3]. In fact, the Council Directive 2013/59/Euratom [4] emphasizes the need for justification and optimization of medical exposures. Regarding the CT contribution within the PET/CT procedure, the Euratom principles entail a thorough justification of the intended use of CT in conjunction with PET image, and the optimization of radiation dose for that purpose.

Three categories, with different levels of radiation dose, have been suggested [5–7]:

- CT for attenuation correction (*AC CT*): provides only a gross delimitation of tissues in order to create the μ-map that quantifies photon losses within the patient. This μ-map is essential to reconstruct the PET image corrected for attenuation effects.
- CT for attenuation correction and anatomical localization (*AC&L CT*): allows the visualization of morphological and anatomical

* Corresponding author at: Clínica Universidad de Navarra, 36, Pío XII Avenue, 31008 Pamplona, Spain.
E-mail address: mjgarciave@unav.es (M.J. García-Velloso).

https://doi.org/10.1016/j.ejmp.2021.03.019
Received 21 September 2020; Received in revised form 22 February 2021; Accepted 13 March 2021
Available online 31 March 2021
1120-1797/© 2021 Associazione Italiana di Fisica Medica. Published by Elsevier Ltd. This is an open access article under the CC BY-NC-ND license (http://creativecommons.org/licenses/by-nc-nd/4.0/).

structures with enough spatial resolution to precise the localization and the extent of PET findings.

- *Diagnostic* CT (*Dx CT*): as CT is also intended for dedicated radiological interpretation, it should be protocoled using established radiology guidelines, regarding the extent of the coverage and the possible use of contrast media. If this diagnostic CT is contrast-enhanced or covers a limited specific region, the acquisition of an additional *AC CT* for attenuation correction should be considered.

For a whole-body PET/CT examination (either oncology, infection or inflammation purpose), the most frequent CT prescription is an *AC&L CT* with sufficient image quality to enable anatomical localization of PET findings, as well as attenuation correction. In fact, in a survey performed in UK [8] comprising 33 PET/CT systems, 76% of the registered examinations turned out to belong to *AC&L CT* category. In this survey [6,8], median radiation dose for a PET/CT was 32% and 45% higher for *AC&L CT* and *Dx CT*, respectively, as compared to an *AC CT*.

In order to minimize radiation dose and maximize diagnostic information, any PET/CT prescription for a particular indication might require a specific protocol. Acquisition parameters such as the extent of the coverage, the radiotracer activity, the PET acquisition time and, obviously, the category of CT should be customized for each indication [9]. Special consideration should be given to those clinical scenarios that may require repeated PET/CT scans in a short-time interval, such as follow-up, clinical trials or multi-tracer protocols. In these cases, CT of some of the PET/CT acquisitions may be redundant concerning anatomical localization or diagnosis, and may be used only for generating the μ-map (*AC CT*).

As an example, within the context of a research project in our PET department, a dual tracer PET/CT scan was performed within a 24 h interval for patients with multiple myeloma [10]. Additionally, following the International Myeloma Working Group recommendations [11], these patients were also prescribed a whole-body low dose CT (WBLDCT) for the assessment of bone infiltration. For the scope of optimization, the dual tracer PET/CT protocol and the WBLDCT were merged in a one-stop-shop. Thus, the CT acquired with the ^{18}F-fluorodeoxyglucose (FDG) PET/CT was also dedicated to radiological diagnosis of bone disease (WBLDCT), while the ^{11}C-methionine (MET) PET/CT was programmed with less radiation dose just for attenuation correction of PET data (*AC CT*), and can be referred as *whole-body ultra-low dose CT* (WBULDCT).

The main objectives of this study were to experimentally determine the minimum level of CT radiation dose than can ensure an accurate attenuation map for PET reconstruction and to quantify the benefit of replacing the standard *Dx CT* procedure by an *AC CT* protocol in a series of patients who underwent a dual tracer PET/CT procedure.

Materials and methods

Images were acquired on a Siemens Biograph mCT PET/CT tomograph (Siemens Medical Solutions, Hoffman States, IL) equipped with a 64 slice Definition AS CT and a LSO PET with extended (21.8 cm) axial field of view [12].

Phantom experiments

The NEMA image quality phantom simulating a human torso and containing 6 coplanar spheres (internal diameters: 10, 13, 17, 22, 28 and 37 mm) and a cylindrical lung insert (diameter 50 mm, approximately) was imaged within a parallelepiped container filled with non-radioactive water (Fig. 1). The area of the cross section filled with water (considering both NEMA phantom and container) was 719 cm^2 and the corresponding effective diameter calculated as proposed by the AAPM is 30.2 cm [13]. The torso phantom background compartment (9600 mL approximately) was filled with a ^{18}F solution of 3.8 kBq/ml and the spheres were filled with a ^{18}F solution of 35.6 kBq/ml (spheres-to-background ratio 9:1) and radiological contrast (300 mg/ml iodine) at 3% dilution. The radiological contrast was introduced in order to mimic high-attenuation structures such as bones .

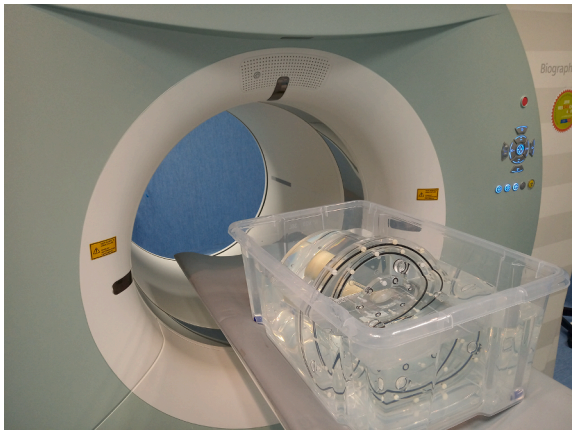

Fig. 1. Experimental setting for NEMA image quality phantom acquisition.

Phantom was imaged within a single bed position. Twenty-one CT images were acquired, with the following common settings: rotation speed at 0.5 sec, collimation of 16x1.2 mm and pitch at 1. Different voltage (80, 100, 120 kV) and current–time product (10, 20, 40, 60, 80, 100, 120 mAs) were programmed. Automatic exposure control (AEC, "CARE Dose" package by Siemens) was disabled in order to acquire with the widest possible range of radiation dose condition. Volume CT dose index for a 32 cm phantom ($CTDI_{vol}$) values were registered for each acquisition condition. CT images were reconstructed with filtered back projection (iterative reconstruction is not supported by our system), a B19f convolution kernel and a slice thickness of 5.0 mm (standard reconstruction for μ-map derivation).

A 10-minute PET acquisition was performed to ensure higher counting statistics than clinical PET scans. PET raw data were reconstructed with each of the 21 CT scans, using the standard reconstruction parameters for oncology scans and accredited by the EANM/EARL programme [14]: iterative algorithm (3 iterations and 21 subsets) with time of flight (TOF), a Gaussian filter of 5.0 mm and a matrix size of 200 × 200. Thus, the only difference between reconstructed PET images was which CT was used for attenuation correction.

All the CTs, attenuation maps (μ-maps) and PET images were visually inspected to identify potential artifacts and quantified to evaluate image quality. Phantom images were analysed using the PMOD software package (version 3.0; PMOD Technologies Ltd, Zurich, Switzerland). Spherical volumes (VOIs) having the same size as the inner diameter of the target sphere were drawn on each sphere. An additional spherical 40

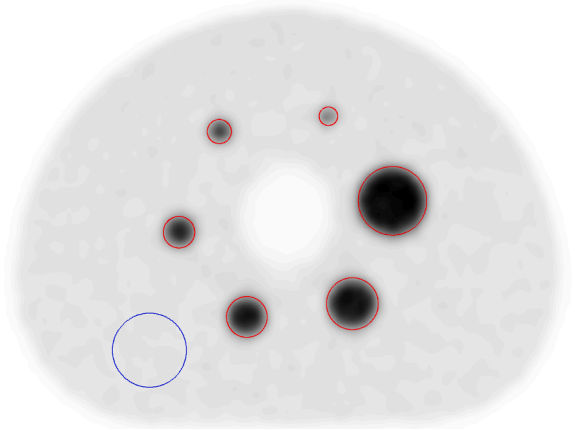

Fig. 2. Volumes of interest used for quantitative analysis.

mm diameter VOI was drawn on the background (Fig. 2), placed intentionally in the most affected area within the image according to a preliminary visual analysis. For each VOI, mean voxel value and standard deviation (SD) were determined both in CT (Hounsfield units, HU) and in μ-map (cm^{-1}). For PET, maximum and mean values (within a 50% isocontour) of radioactivity concentration (kBq/cc) were obtained in the spheres, while mean and standard deviation were calculated for the background.

In order to accept a CT image for PET reconstruction, two major issues must be preserved in comparison with a standard *AC&L CT*: PET image quality (noise level and/or presence of artifacts) and accurate quantification of PET images. Hence, specific analysis of phantom images was designed to test these two problems:

- Image quality: Noise level was analysed by measuring the coefficient of variation (COV) (%) in the background of the three sets of images (CT, μ-map and PET) and also within the spheres in CT and μ-map. Noise measurements in high uptake objects were not evaluated in PET images, as they would be affected by partial volume effects [15]. As mean value of the background in the CT image is around 0 HU, COV takes very high values (range ± 10^4) and could neither be analysed.

$$COV_{VOI}(\%) = 100 \cdot \frac{SD_{VOI}}{Mean_{VOI}}$$

- Quantification: In the μ-maps, mean attenuation coefficient in the areas with contrast and water were quantified. For PET images, activity concentration recovery coefficients were calculated as the mean or maximum VOI concentration normalized by the actual activity concentration in the spheres [7].

$$RC_{mean}(\%) = 100 \cdot \frac{Mean_{VOI}}{Actual\ concentration}$$

$$RC_{max}(\%) = 100 \cdot \frac{Max_{VOI}}{Actual\ concentration}$$

All data were compared to values obtained with the highest dose CT (*120 kV-120mAs*):

$$Difference(\%) = 100 \cdot \frac{Value_{xkV-ymAs} - Value_{120kV-120mAs}}{Value_{120kV-120mAs}}$$

Patients

A total of 31 adult patients with histologically proven multiple myeloma who had been enrolled in a research project (PI16-00225 Carlos III Health Institute, Spain) were retrospectively reviewed for radiation dose evaluation. All patients had signed an informed consent and had agreed to undergo a standard PET/CT with FDG and an investigational PET/CT with MET, as approved by the Research Ethics Committee of Clínica Universidad de Navarra (161/2015). The retrospective review of radiation dose was also approved by our Research Ethics Committee (161/2019) but the need for informed consent was waived.

Both PET/CT studies, with FDG and MET, covered the whole skeleton from head to feet, with patients in supine position and with the arms beside the body. The CT for FDG was programmed as a standard WBLDCT for radiological diagnosis (tube voltage of 120 kV, 80 mAs reference and AEC), while the CT for MET was aimed only for attenuation correction purpose and will be referred as WBULDCT (100 kV, 40 mAs reference, with AEC). Both CT acquisition were performed with rotation speed of 0.5 s, pitch 1 and collimation of 16x1.2 mm, without any contrast agents. From each CT raw data, the standard reconstruction for attenuation correction was performed with filtered back projection, a B19f convolution kernel and a slice thickness of 5.0 mm. Additional reconstructions of the WBLDCT were programmed for radiological diagnosis, also with filtered back projection but with sharper filters (B40f or B60f), thinner slices (2.0 or 3.0 mm) and different orientations (coronal or sagittal). Reconstructed μ-maps were not available for retrospective review, since only CT images reconstructed for clinical evaluation are routinely achieved in the PACS system. For each patient, the same number of bed positions were acquired in both PET/CT exams (12 to 15) depending on patient's height. PET acquisitions were performed according to our standard protocol for oncological studies (2 min per bed position, EARL reconstruction). Then, a nuclear medicine physician (MJGV) reported PET findings of both PET scans and a radiologist (JDA) reported CT findings on the WBLDCT.

Demographic data of the patients (age, sex, height, weight and body mass index (BMI)) and volume CT dose index ($CTDI_{vol}$) and dose-length product (DLP) were recorded. Effective doses from the CT component were calculated with CT-Expo software (version 2.4) using ICRP-103 tissue weighting factors and patient $CTDI_{vol}$ and DLP as input magnitudes. This software provides gender-specific dose calculation, based on the adult female model EVA and male model ADAM. The administered radiotracer activity was also registered and its corresponding radiation dose was calculated by multiplying the injected activity by the dose coefficient for each radiopharmaceutical based on ICRP-103 tissue weighting factors (0.0159 mSv/MBq for FDG and 0.00549 mSv/MBq for MET [16]).

Despite the fact that WBULDCT was intended nor for diagnosis neither for anatomical localization, and that image quality was not the priority aim, a retrospective evaluation of these images was performed in order to investigate if image quality was still acceptable for bone assessment and if, thus, there would exist scope for further optimization of the WBLDCT scan. To this aim, lytic lesions greater than 5 mm (maximum axial diameter) described in the radiologist clinical report based on the WBLDCT image were listed. In patients with multiple findings, two representative lesions per anatomic area (skull, vertebral column, thoracic cage, pelvic bones and long bones) were selected. Subsequently, when all the patients were scanned and elected for this project, a non-blinded retrospective review of the WBULDCT was performed by the radiologist, in order to evaluate the detectability of every registered focal lesion.

Statistical analysis

Statistical analysis was performed using STATA version 12 (StataCorp LP, College Station, Texas, USA). A Shapiro-Wilk test was used to test for normal distribution. Data following normal distribution are given as mean ± standard deviation (SD) and non-normally distributed data as median and interquartile range (IQR). For non-normal variables, pairwise comparisons were evaluated using the sign test, and correlations were tested using the Spearman rank correlation coefficient.

Results

Phantom experiments

Table 1 shows $CTDI_{vol}$ values, which ranged from 0.2 to 8.7 mGy. CT, μ-map and PET images are presented in Fig. 3 for visual analysis. An evident artifact is visible both in CT and μ-map for the two lowest $CTDI_{vol}$ conditions (*80 kV-20mAs* and *80 kV-10mAs)*. However,

Table 1
$CTDI_{vol}$ values (mGy) of the 21 CT acquisitions of the NEMA phantom.

	80 kV	100 kV	120 kV
10 mAs	0.20	0.43	0.73
20 mAs	0.41	0.86	1.46
40 mAs	0.82	1.72	2.91
60 mAs	1.23	2.58	4.37
80 mAs	1.63	3.42	5.79
100 mAs	2.04	4.28	7.24
120 mAs	2.45	5.14	8.70

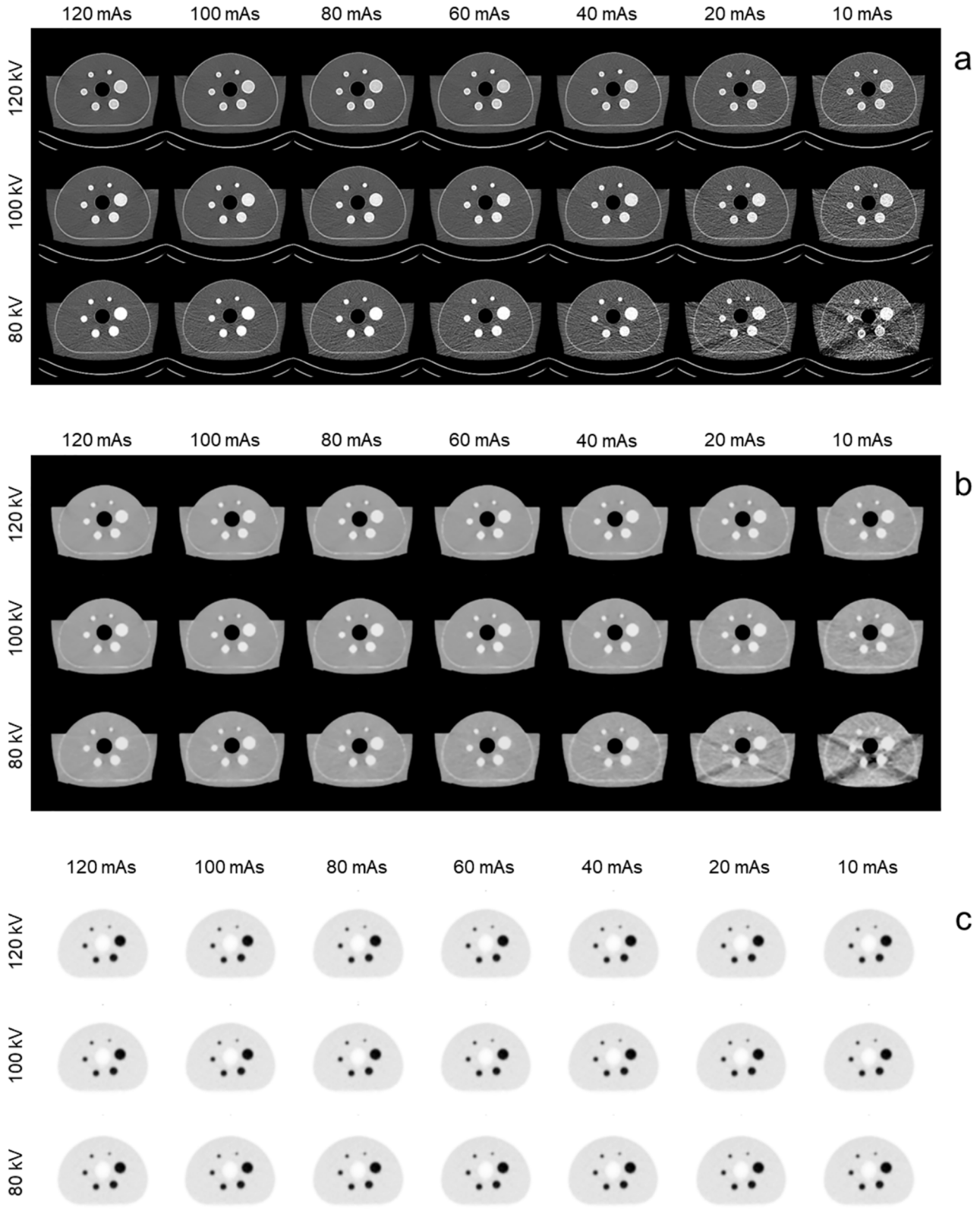

Fig. 3. CT (a), μ-map (b) and PET (c) images obtained with the 21 different CT acquisition parameters.

subsequent PET images seem to be unaffected by that artifact in the μ-map. Aside from the artifact, CT images show higher noise level as $CTDI_{vol}$ is reduced. However, this effect is not visually perceived on the μ-maps. All PET images look very similar, independently of which μ-map was used in the reconstruction.

VOIs used to quantify the images were presented in Fig. 2. It should be noticed that background VOI was intentionally placed within the artifact in order to analyse the worst scenario.

Regarding noise level and considering all radiation dose conditions, COV in the CT images was 49.8 ± 9.3% within the spheres, while COV in the μ-map was 0.42 ± 0.22% within the spheres and 0.41 ± 0.54% in the background. When the influence of this noise is evaluated in PET data,

noise measured in the reference reconstruction (*120 kV-120mAs*) was considered as reference (COV in the background 6.6%). PET COV measured in the other conditions differed<0.7% respect to the reference, except for the *80 kV-10mAs* condition in which difference increased up to 2.53%. Therefore, noise in PET images barely varies across conditions.

Fig. 4.A presents percentage differences obtained in μ coefficients both in background and spheres when compared to the reference μ values obtained with the highest dose condition (*120 kV-120mAs*). All the differences lay within ± 1%, except for one data in the background, particularly, the measurement with the *80 kV-10mAs* acquisition, where the artifact is clearly affecting the quantification.

Differences in recovery coefficients as a function of sphere diameter are presented in Fig. 4.B and Fig. 4.C. All percentage differences between each recovery coefficient and its corresponding reference value (*120 kV-120 mAs*) fall within the range of [-0.72; 1.66] % for RC_{mean} and [-1.42; 1.69] % for RC_{max}. When the two qualitatively worst conditions were disregarded, the range is reduced to [-0.59; 1.06] % for RC_{mean} and [-0.56; 1.12] % for RC_{max}.

Patients

In this retrospective study, data of 31 patients, 23 males and 8 females, aged 59 ± 10 years were analysed. In this series, weight was 77.8 ± 14.5 kg, height was 169.3 ± 9.8 cm, and BMI was 27.0 ± 3.8 kg/m^2. There were statistically significant differences among males and females in weight (*t*-test, $p < 0.05$) and height (*t*-test, $p < 0.05$) but not in BMI (*t*-test, $p = 0.22$).

Table 2 shows effective mAs, $CTDI_{vol}$, DLP, and effective dose values as median (IQR) for both CT acquisitions: WBLDCT and WBULDCT. Non-parametric sign test demonstrated pairwise statistical differences in mAs, $CTDI_{vol}$, DLP and effective dose ($p < 0.0001$). Dose indexes of *WBULDCT* and *WBLDCT* were highly correlated. As shown in Fig. 5, median effective dose was reduced from 6.4 mSv to 2.1 mSv, which means a median radiation dose reduction of 66.7% when substituting a WBLDCT by a WBULDCT.

The relationship between DLP and the effective dose derived by CT-Expo software was adjusted to a linear equation with zero intercept, in order to calculate a k-factor for easing prospective calculations of effective dose. The resultant k-factor was 0.00801 mSv/mGy·cm for men (N = 46) and 0.00968 mSv/mGy·cm (N = 16) for women, with R^2 greater than 0.999 and $p < 0.001$ for both cases. Therefore, same DLP values seem to cause 20.8% higher effective dose to females than to males.

Patients were administered 327 ± 75 MBq of FDG and 469 ± 50 MBq of MET. Resultant effective doses were 5.2 ± 1.2 mSv and 2.6 ± 0.3 mSv, respectively. In the FDG PET/CT, radiation dose due to the PET tracer is lower than the radiation dose due to the CT part while in MET PET/CT tracer radiation dose is higher than the CT contribution (Fig. 5). Total effective dose for each PET/CT was 11.7 ± 2.8 mSv for FDG and 4.8 ± 0.7 mSv for MET. It should be noted that the additional study (MET PET/CT) for the research project conducted at our institution yielded approximately a 40% additional radiation dose respect to standard examination for this indication (FDG PET/CT).

Table 2
CT acquisition parameters and effective dose for WBLDCT and WBULDCT and statistical analysis.

Protocol	Effective mAs	$CTDI_{vol}$ (mGy)	DLP (mGy·cm)	Effective dose (mSv)
WBLDCT	58 (IQR: 18)	4.2 (IQR: 1.4)	790 (IQR: 282)	6.4 (IQR: 2.0)
WBULDCT	33 (IQR: 14)	1.2 (IQR: 0.58)	262 (IQR: 123)	2.1 (IQR: 0.8)
Wilcoxon test	$p < 0.0001$	$p < 0.0001$	$p < 0.0001$	$p < 0.0001$
Spearman test	$\rho = 0.88$ ($p < 0.0001$)	$\rho = 0.89$ ($p < 0.0001$)	$\rho = 0.92$ ($p < 0.0001$)	$\rho = 0.90$ ($p < 0.0001$)

Example CT images are presented in Fig. 6, where WBULDCT shows clearly degraded image quality especially in soft tissue. However, it provides sufficient information to warrant a thorough bone structures review. The μ-maps are intensely smoothed as compared to the initial CT image, demonstrating that a noisy image is undoubtedly acceptable for accurate attenuation correction.

In the total series, there were 3 patients with diffuse bone marrow infiltration but no lytic lesions. A total of 115 lytic lesions were reported by the radiologist in the *WBLDCT* and, in the retrospective review, only 6 out of 115 lesions (5.2%) were unidentifiable in the *WBULDCT*. Non-detected lesions were either smaller than 10 mm or related to high bone demineralization (see Fig. 7). Even though most lesions were detectable by the radiologist, the presence of noise and artifacts hampered image reading.

Discussion

This study aims to describe a practical example of radiation dose optimization in the clinical arena. The first part of this research has demonstrated, with phantom experiments, that low dose CT is suitable to generate an accurate μ-map without any qualitative or quantitative distortion of PET image. The second one deals with an optimized PET/CT protocol in which a *WLULDCT* dedicated just for attenuation correction was introduced, achieving an important reduction of patients' radiation dose.

Regarding phantom experiments, some ideas should be discussed. Although numerous publications are focused on CT for attenuation correction, most of them are based on simulations [17–20]. Among the papers based on phantoms [21–23], the present study is, to our knowledge, the first one to include hot spheres to ensure accurate quantitation of high uptake lesions, radiological contrast to mimic high-

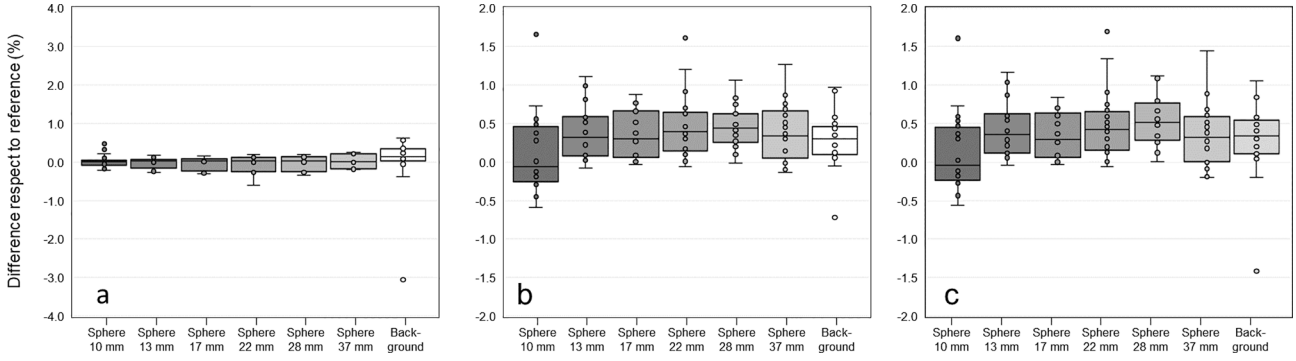

Fig. 4. Box plot of the differences observed in comparison to the reference *120 kV-120mAs* condition: a) μ coefficients in each attenuation map; b) RC_{mean} on the spheres and the background in each PET reconstruction; c) RC_{max} on the spheres and the background in each PET reconstruction.

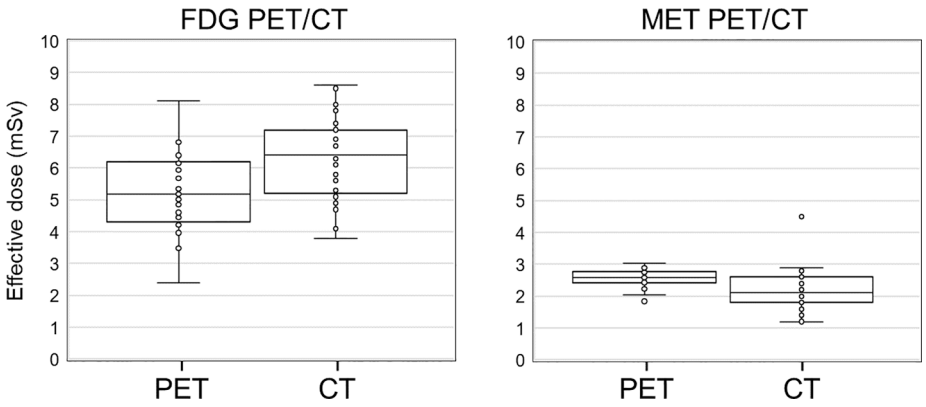

Fig. 5. Effective doses received by the patients in FDG and MET PET/CT, both due to the PET radiopharmaceutical and to the CT component.

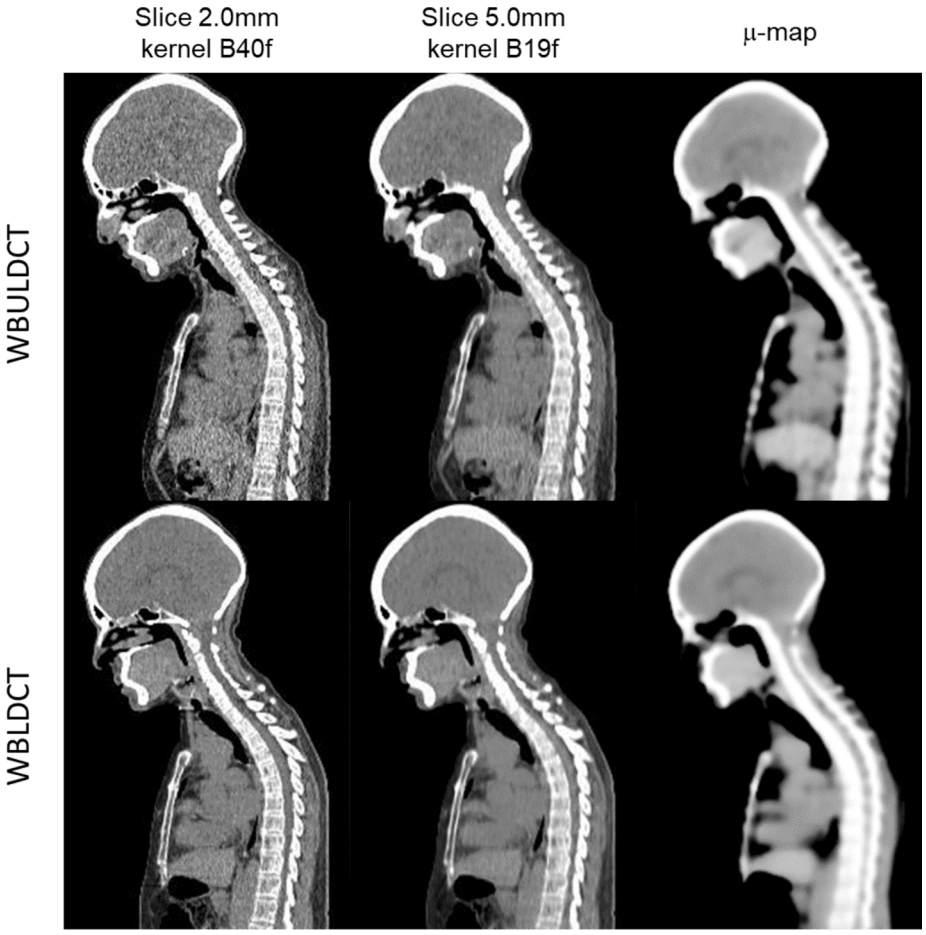

Fig. 6. Example images of WBLDCT and WBULDCT for a patient. Images on the left are reconstructed for anatomical localization and diagnosis (this reconstruction is not routinely performed in the WBULDCT and is presented just for comparison purposes); images on the middle are reconstructed for μ-map derivation; and images on the right represent the final μ-maps. All the images are presented with soft tissue windowing.

attenuation structures such as bones and a large container to increase photon attenuation. To this respect, the effective diameter of our setting could be introduced in the equation inferred by O'Neill *et al.* [24] to estimate the body habitus mimicked by the phantom. BMI was calculated as 27.4 kg/m^2, and, therefore, phantom might simulate the attenuation of an overweight patient.

Noise observed in the anthropomorphic phantom CT images is clearly higher than that of the μ-maps and corrected PET images. The impact of CT image noise in the final reconstructed PET image is mitigated due to both, the down-sampling and smoothing of the CT prior to the μ-map generation, and the integration of voxels along the line of response in order to apply the μ-map to the raw PET data [25,26]. Therefore, PET quality seems to be unaffected by apparent CT image quality, except when large artifacts appear.

Most of the CT images produced proper μ-maps with PET quantification deviations lower than ± 1.2%, except for those with $CTDI_{vol}$ lower than 0.43 mGy and the the cross-shaped artifact. A similar artifact has been previously described by Colsher et al. [21]. These authors explain that, as μ coefficient is proportional to the negative logarithm of the raw counts, μ calculation fails if there are any negative values in the

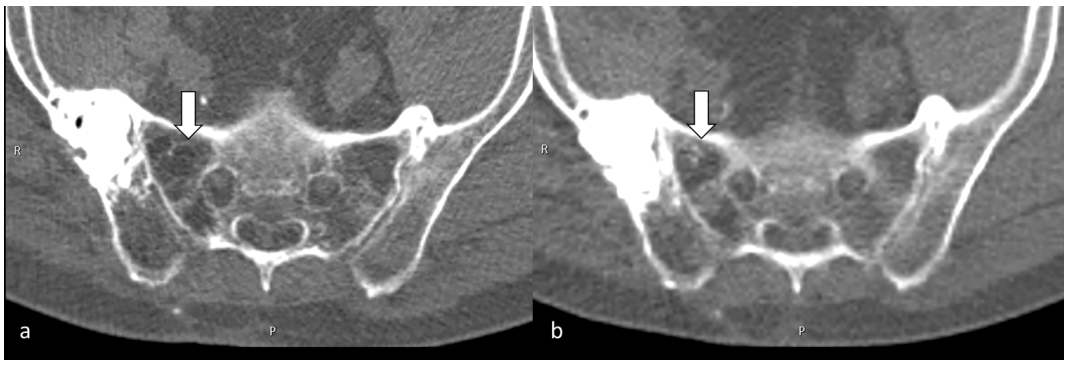

Fig. 7. Study in a 68-year-old male with multiple myeloma and bone destruction in the pelvis: (a) WBLDCT and (b) WBULDCT. A lytic lesion in the right sacral wing of S1 with septa that delimits the lesion (see arrow) is present in WBLDCT (a). At WBULDCT axial image (b) the septa are not visible and the bone structure is quite similar to the left sacral wing (see arrow).

projection data. Unfortunately, we have been unable to access the raw CT data to check this point. Taking into account the results by Ho Shon *et al.* [23], who demonstrated that PET quantification is preserved when $CTDI_{vol}$ is greater than 1 mGy, a $CTDI_{vol}$ of 1 mGy is recommended as a conservative lower limit for accurate attenuation correction and PET quantification.

Phantom experiments have demonstrated that PET recovery coefficients vary<2% in the whole set of PET images, when reconstructed with different μ-maps. This variation can be considered negligible, taking into account the uncertainties involved in PET imaging [7]. In fact, the accreditation programme of the European Association of Nuclear Medicine [7,14] establishes an acceptance of ± 10% for calibration.

Focusing in the clinical application of this research, we decided to implement the *AC CT* in our PET department for multiple myeloma PET protocol. This indication was chosen since patients were explored twice in a very short time period with a total body scan coverage and they would have a great benefit in terms of radiation dose. In light of the experimental results and taking into account that AEC is always active in clinical patients, physicians agreed to modify the protocol in clinical routine as long as kV was preserved at 100 kV and reference mAs was set to 40 mAs. Although this protocol does not represent the lowest dose achievable according to phantom experiments, it yielded to a great dose reduction preserving relevant diagnostic information. Our approximation differs from Fahey et al. [22] recommendations, who proposed to maintain tube voltage at 120 kVp and to use the lowest tube current–time product setting (5 mAs). Nai et al. [27] have also proposed a low dose PET/CT protocol for lung cancer screening with reduced current–time product (from 140 mAs to 40 mAs with CAE) but tube voltage fixed at 120 kV. However, in our experience, the reduction of tube voltage from 120 kV to 100 kV achieves a significant $CTDI_{vol}$ reduction without any image degradation. On the other hand, we have preferred not to reduce current–time product to the lowest value and to maintain AEC instead, due to the fact that uniform image quality is desired for the whole axial coverage.

In our series, median current–time product for the WBULDCT was 33.0 (IQR: 14.0) mAs and median dose was 2.1 (IQR: 0.8) mSv. Although the modern paradigm of CT dose optimization is to achieve a sub-millisievert protocol [28,29], our WBULDCT protocol has finally doubled that level. It should be noted that a sub-millisievert CT might be unrealistic for an exploration from head to feet without the state-of-art tools for radiation dose reduction and image quality improvement (spectral filtration and iterative reconstruction). Taking into account that reduced kV could introduce artifacts in the attenuation map (Fig. 3), the only feasible way to achieve the sub-millisievert target would be to further reduce the current–time product [25]. We are now considering this modification for future studies. Despite the low dose and the limited image quality, most radiological findings were identifiable thanks to the high intrinsic contrast of bone tissue.

Regarding the WBLDCT, the first optimization decision was to merge the nuclear medicine exploration and the radiological examination, with an evident benefit for patients in terms of time and radiation dose. In order to fix the acquisition parameters, we reviewed the protocol of WBLDCT for multiple myeloma and found some variations from site to site: 120 kV and 40 mAs without AEC [30,31]; 120 kV and 70 reference mAs with AEC [32]; 100 kV and 111 reference mAs with AEC [33]. Finally, we decided to follow the recommendations from Moulopoulos et al. [34] of using a 120 kV voltage and a time–current product between 50 and 70 mAs. In our cohort, even though the reference mAs was set to 80 mAs, final median current–time product was 58.0 (IQR: 18.0) mAs and median effective dose was 6.4 (IQR: 2.0) mSv. The effective dose of our WBLDCT seems to be slightly higher as compared to other publications: 4.2 mSv [31], 3.2 mSv [30], 5.65 mSv [33] and 4 to 5 mSv depending on the tomograph model [32]. Differences can be partially attributed to different methods for effective dose calculation (Radimetrics was used by Hemke et al. [32]) or different extent of coverage (head to feet in our case). However, we should also anticipate that there might be scope for further dose reduction. It should be also noted that the CT scanner in the Siemens mCT PET/CT tomograph does not enable spectral shaping or iterative reconstruction. These techniques have proven a significant reduction in WBLDCT radiation exposure [33], achieving 1.45 mSv in a third generation CT tomograph. Additionally, tin filtrated CT available in the newest CT scanner models might play an important role in the diagnosis and management of multiple myeloma at very low radiation dose (<1 mSv) [35]. However, the suitability of this tin filtrated CT for accurate PET attenuation correction has not been demonstrated yet.

Regarding the effective dose calculation, we have used CT-Expo calculator that provides gender-specific calculations. We consider that the main limitation of this software is that AEC is only simulated using a standard profile to account for the effects of longitudinal and 3D dose modulation as a rough approximation. From our data, we have derived the gender-specific k-factors for prospective dose calculations, obtaining 0.00801 mSv/mGy·cm for men and 0.00968 mSv/mGy·cm for women. We have obtained a 20.8% higher k-factor for females than for males, in agreement with data published by Cretti and Perugini [30]. According to these results, the use of the standard factor for head and torso (0.015 mSv/mGy·cm [36,37]) for CT studies including limbs may lead to large overestimation of final effective dose [33]. The k-factor for a CT covering from head to feet has been recently investigated by Inoue et al. [38], who noticed a significant dependence on the AEC model. These authors obtained a conversion coefficient of 0.0100 mSv/mGy·cm when AEC is based on the AP scout, being in agreement with our estimation.

Certain limitations of our study need to be pointed out. First of all, image quality of clinical PET images obtained with WBULDCT and WBLDCT could not be objectively compared because PET image quality

was mainly related to the tracer distribution, and we were not able to isolate the influence of the μ-map. In addition, WBLDCT and WBULDCT had different reconstruction settings with different slice thickness and filters, and noise in the final image was not objectively evaluated as it would be greatly influenced by the reconstruction parameters and not only by acquisition conditions. Another limitation of our study is the simplified approach that we used to estimate PET effective dose. However, this approximation has been considered suitable in previous publications [39]. Besides, since CT-Expo is based on the standard adult model without considering body habitus, CT dose values could be overestimated for overweight patients. Finally, the evaluation of the detectability of lytic lesions in WBULDCT images was roughly addressed. Clinical reports were retrospectively reviewed to register lesions detected in the WBLDCT and, subsequently, a non-blinded evaluation of each lesion in the WBULDCT was conducted. It should be noted that this non-rigorous analysis did not intend to meticulously evaluate image quality or diagnostic performance, but only aimed to know radiologist's judgement in order to consider a further optimization of the WBLDCT.

Conclusion

Accurate attenuation of PET images can be precisely measured with a very low dose CT acquisition. We optimized the CT radiation dose in a dual tracer PET/CT protocol. We have demonstrated that an effort in reviewing each PET/CT indication could lead to optimization of the protocol for specific pathologies and clinical indications, with the subsequent dose reduction.

References

[1] Mettler FA, Bhargavan M, Faulkner K, Gilley DB, Gray JE, Ibbott GS, et al. Radiologic and nuclear medicine studies in the united states and worldwide: frequency, radiation dose, and comparison with other radiation sources - 1950–2007. Radiology 2009;253(2):520–31. https://doi.org/10.1148/radiol.2532082010.

[2] Mettler FA, Mahesh M, Bhargavan-Chatfield M, Chambers CE, Elee JG, Frush DP, et al. Patient exposure from radiologic and nuclear medicine procedures in the united states: procedure volume and effective dose for the period 2006–2016. Radiology 2020;295(2):418–27. https://doi.org/10.1148/radiol.2020192256.

[3] Parisi MT, Bermo MS, Alessio AM, Sharp SE, Gelfand MJ, Shulkin BL. Optimization of pediatric PET/CT. Semin Nucl Med 2017;47(3):258–74. https://doi.org/10.1053/j.semnuclmed.2017.01.002.

[4] The council of the european union. Council Directive 2013/59/EURATOM. Laying down basic safety standards for protection against the dangers arising from exposure to ionising. Off J Eur Union 2013:1–73.

[5] Brady SL, Shulkin BL. Dose optimization: a review of CT imaging for PET attenuation correction. Clin Transl Imaging 2017;5(4):359–71. https://doi.org/10.1007/s40336-017-0232-0.

[6] Salvatori M, Rizzo A, Rovera G, Indovina L, Schillaci O. Radiation dose in nuclear medicine: the hybrid imaging. Radiol Med 2019;124(8):768–76. https://doi.org/10.1007/s11547-019-00989-y.

[7] Boellaard R, Delgado-Bolton R, Oyen WJG, Giammarile F, Tatsch K, Eschner W, et al. FDG PET/CT: EANM procedure guidelines for tumour imaging: version 2.0. Eur J Nucl Med Mol Imaging 2015;42(2):328–54.

[8] Iball GR, Bebbington NA, Burniston M, Edyvean S, Fraser L, Julyan P, et al. A national survey of computed tomography doses in hybrid PET-CT and SPECT-CT examinations in the UK. Nucl Med Commun 2017;38:459–70. https://doi.org/10.1097/MNM.0000000000000672.

[9] Bertolini V, Palmieri A, Bassi MC, Bertolini M, Trojani V, Piccagli V, et al. CT protocol optimisation in PET/CT: a systematic review. EJNMMI Phys 2020;7(1). https://doi.org/10.1186/s40658-020-00287-x.

[10] Lapa C, Garcia-Velloso MJ, Lückerath K, Samnick S, Schreder M, Otero PR, et al. 11C-Methionine-PET in multiple myeloma: a combined study from two different institutions. Theranostics 2017;7(11):2956–64. https://doi.org/10.7150/thno.20491.

[11] Rajkumar SV, Dimopoulos MA, Palumbo A, Blade J, Merlini G, Mateos M-V, et al. International myeloma working group updated criteria for the diagnosis of multiple myeloma. Lancet Oncol 2014;15(12):e538–48. https://doi.org/10.1016/S1470-2045(14)70442-5.

[12] Martí-Climent JM, Prieto E, Domínguez-Prado I, García-Velloso MJ, Rodríguez-Fraile M, Arbizu J, et al. Contribution of time of flight and point spread function modeling to the performance characteristics of the PET/CT biograph mCT scanner. Rev Esp Med Nucl Imagen Mol 2013;32:13–21. https://doi.org/10.1016/j.remn.2012.07.001.

[13] Medicine AA of P in. Size-specific dose estimates (SSDE) in pediatric and adults body CT examinations 2011:634. https://www.aapm.org/pubs/reports/RPT_204.pdf.

[14] Kaalep A, Sera T, Oyen W, Krause BJ, Chiti A, Liu Y, et al. EANM/EARL FDG-PET/CT accreditation - summary results from the first 200 accredited imaging systems. Eur J Nucl Med Mol Imaging 2018;45(3):412–22. https://doi.org/10.1007/s00259-017-3853-7.

[15] Association NEM. NEMA NU 2–2012 performance measurements of positron emission tomographs. VA: Rosslyn; 2012.

[16] Andersson M, Johansson L, Minarik D, Leide-Svegborn S, Mattsson S. Effective dose to adult patients from 338 radiopharmaceuticals estimated using ICRP biokinetic data, ICRP/ICRU computational reference phantoms and ICRP 2007 tissue weighting factors. EJNMMI Phys 2014;1:1–13. https://doi.org/10.1186/2197-7364-1-9.

[17] Xia T, Alessio AM, Alessio AM, De Man B, Manjeshwar R, Asma E, et al. Ultra-low dose CT attenuation correction for PET/CT. Phys Med Biol 2012;57:309–28. https://doi.org/10.1088/0031-9155/57/2/309.

[18] Rui X, Cheng L, Long Y, Fu L, Alessio AM, Asma E, et al. Ultra-low dose CT attenuation correction for PET/CT: analysis of sparse view data acquisition and reconstruction algorithms. Phys Med Biol 2015;60(19):7437–60. https://doi.org/10.1088/0031-9155/60/19/7437.

[19] Miao J, Fan J. A practical sparse-view ultra-low dose CT acquisition scheme for PET attenuation correction. 2015 IEEE Nucl. Sci. Symp. Med. Imaging Conf., IEEE; 2015, p. 1–2. https://doi.org/10.1109/NSSMIC.2015.7582031.

[20] Abella M, Alessio AM, Mankoff DA, MacDonald LR, Vaquero JJ, Desco M, et al. Accuracy of CT-based attenuation correction in PET/CT bone imaging. Phys Med Biol 2012;57(9):2477–90. https://doi.org/10.1088/0031-9155/57/9/2477.

[21] Colsher JG, Hsieh J, Thibault JB, Lonn A, Pan T, Lokitz SJ, et al. Ultra low dose CT for attenuation correction in PET/CT. IEEE Nucl Sci Symp Conf Rec 2008:5506–11. https://doi.org/10.1109/NSSMIC.2008.4774499.

[22] Fahey FH, Palmer MR, Strauss KJ, Zimmerman RE, Badawi RD, Treves ST. Dosimetry and Adequacy of CT-based attenuation correction for pediatric PET: phantom study. Radiology 2007;243(1):96–104. https://doi.org/10.1148/radiol.2431060696.

[23] Ho Shon I, Reece C, Hennessy T, Horsfield M, McBride B. Influence of X-ray computed tomography (CT) exposure and reconstruction parameters on positron emission tomography (PET) quantitation. EJNMMI Phys 2020;7:1–16. https://doi.org/10.1186/s40658-020-00331-w.

[24] O'Neill S, Kavanagh RG, Carey BW, Moore N, Maher M, O'Connor OJ. Using body mass index to estimate individualised patient radiation dose in abdominal computed tomography. Eur Radiol Exp 2018;2(1). https://doi.org/10.1186/s41747-018-0070-5.

[25] Siemens Healthineers. Dose reduction techniques for CT-based PET attenuation correction. Tech White Pap n.d.

[26] Fahey FH, Goodkind A, MacDougall RD, Oberg L, Ziniel SI, Cappock R, et al. Operational and dosimetric aspects of pediatric PET/CT. J Nucl Med 2017;58(9):1360–6. https://doi.org/10.2967/jnumed.116.182899.

[27] Nai Y-H, Schaefferkoetter J, Fakhry-Darian D, O'Doherty S, Totman JJ, Conti M, et al. Validation of low-dose lung cancer PET-CT protocol and PET image improvement using machine learning. Phys Medica 2021;81:285–94. https://doi.org/10.1016/j.ejmp.2020.11.027.

[28] Kang HJ, Kim SH, Shin Il C, Joo I, Ryu H, Kim SG, et al. Sub-millisievert CT colonography: effect of knowledge-based iterative reconstruction on the detection of colonic polyps. Eur Radiol 2018;28(12):5258–66. https://doi.org/10.1007/s00330-018-5545-5.

[29] Weinrich JM, Regier M, Well L, Bannas P, Nykolyn O, Heinemann A, et al. Feasibility of sub-milliSievert CT of the cervical spine: Initial results in fresh human cadavers. Eur J Radiol 2019;120:108697. https://doi.org/10.1016/j.ejrad.2019.108697.

[30] Cretti F, Perugini G. Patient dose evaluation for the whole-body low-dose multidetector CT (WBLDMDCT) skeleton study in multiple myeloma (MM). Radiol Medica 2016;121(2):93–105. https://doi.org/10.1007/s11547-015-0573-6.

[31] Ippolito D, Besostri V, Bonaffini PA, Rossini F, Di Lelio A, Sironi S. Diagnostic value of whole-body low-dose computed tomography (WBLDCT) in bone lesions detection in patients with multiple myeloma (MM). Eur J Radiol 2013;82(12):2322–7. https://doi.org/10.1016/j.ejrad.2013.08.036.

[32] Hemke R, Yang K, Husseini J, Bredella MA, Simeone FJ. Organ dose and total effective dose of whole-body CT in multiple myeloma patients. Skeletal Radiol 2020;49(4):549–54. https://doi.org/10.1007/s00256-019-03292-z.

[33] Suntharalingam S, Mikat C, Wetter A, Guberina N, Salem A, Heil P, et al. Whole-body ultra-low dose CT using spectral shaping for detection of osteolytic lesion in multiple myeloma. Eur Radiol 2018;28(6):2273–80. https://doi.org/10.1007/s00330-017-5243-8.

[34] Moulopoulos LA, Koutoulidis V, Hillengass J, Zamagni E, Aquerreta JD, et al. Recommendations for acquisition, interpretation and reporting of whole body low dose CT in patients with multiple myeloma and other plasma cell disorders: a report of the IMWG Bone Working Group. Blood Cancer J 2018;8(10). https://doi.org/10.1038/s41408-018-0124-1.

[35] Boyd C, Hickson K. Radiation dosimetry considerations for skeletal survey imaging of multiple myeloma. Phys Medica 2019;64:109–13. https://doi.org/10.1016/j.ejmp.2019.06.012.

[36] Martí-Climent JM, Prieto E, Morán V, Sancho L, Rodríguez-Fraile M, Arbizu J, et al. Effective dose estimation for oncological and neurological PET/CT procedures. Eur J Nucl Med Mol Imaging Res 2017;7(1). https://doi.org/10.1186/s13550-017-0272-5.

[37] Huda W, Magill D, He W. CT effective dose per dose length product using ICRP 103 weighting factors. Med Phys 2011;38(3):1261–5. https://doi.org/10.1118/1.3544350.

[38] Inoue Y, Nagahara K, Kudo H, Itoh H. Effects of the scan range on radiation dose in the Computed Tomography component of oncology Positron Emission Tomography/Computed Tomography. Radiat Prot Dosimetry 2019;185:1–6. https://doi.org/10.1093/rpd/ncy210.

[39] Prieto E, García-Velloso MJ, Rodríguez-Fraile M, Morán V, García-García B, Guillén F, et al. Significant dose reduction is feasible in FDG PET/CT protocols without compromising diagnostic quality. Phys Medica 2018;46:134–9. https://doi.org/10.1016/j.ejmp.2018.01.021.